AIAA 2001-2460

EXPERIMENTAL INVESTIGATION OF THE FLOW OVER A TOROIDAL AEROCAPTURE BALLUTE

A.Rasheed*, K.Fujii† and H.G.Hornung‡
California Institute of Technology, Pasadena, California, 91125

J.L.Hall§
Jet Propulsion Laboratory, NASA, Pasadena, California, 91109

Abstract

NASA proposals for future planetary spacecraft involve the use of aerocapture to save propellant mass needed to enter planetary orbit. One concept that is being studied uses inflatable structures (ballutes) towed behind the spacecraft to provide the necessary drag while minimizing vehicle heating and flow unsteadiness. Experiments of the tandem body configuration of a toroidal ballute towed behind a spacecraft were performed in the T5 Hypervelocity Shock Tunnel. The test gases studied were carbon dioxide, nitrogen and hydrogen to simulate actual future missions to Mars, Titan and Neptune, respectively. Stagnation point heat transfer measurements were made and were found to compare well with theoretical estimates. In addition, flow visualization shadowgraphs were used to confirm that the flow was steady. The carbon dioxide and nitrogen tests successfully matched both the Reynolds number and enthalpy similarity criteria for the specific NASA missions. The hydrogen shots, however, failed to match the enthalpy criteria for the intended mission and care must be taken when using those results.

1 Introduction

As part of its Solar System Exploration Program, NASA is considering missions to Mars, Titan and Neptune involving the use of aerocapture for orbital insertion. The aerocapturing technique involves skimming the upper atmosphere of the planet and relying on atmospheric drag to slow the spacecraft for capture by the planet's gravity field. This presents numerous technical challenges as the spacecraft must develop a significant amount of drag, while minimizing heat flux and maintaining some margin of control stability. In addition, as with all spacecraft, there are severe mass and volume restrictions. One concept is to inflate a large structure tethered behind the spacecraft to present a large surface area in order to develop the required drag, much like a parachute. This inflatable 'balloon parachute' has been named 'ballute'[6,7].

Computations of the hypersonic flow of a perfect gas over a spacecraft in front of a spherical ballute, using the Euler equation, have shown that the flow becomes violently unsteady, because of the shock–shock interaction where the spacecraft shock impinges on the ballute shock[9]. An attractive alternative is to make the ballute in the form of a torus, so that the spacecraft bow shock is swallowed in the ring and the interaction between the spacecraft and ballute shocks is moved to a region well downstream of the ballute. Further computations showed that such a configuration produces steady flow. The only apparent disadvantage of the toroidal ballute is that the radius of curvature of the ring cross section is quite small, and since the heat transfer rate is proportional to the inverse square root of the radius of curvature, the heat loads on the ring might well be prohibitive. A series of experiments have been performed in the T5 Hypervelocity Shock Tunnel with the aim of determining the heat transfer rates to the ring for flows that approximate similarity with three specific missions in which such a toroidal ballute might be deployed.

2 Hypervelocity Similarity

The relevant parameters in hypervelocity flow are different from the ones that are normally important in other flight regimes because of the high flight velocities (and therefore high total specific enthalpy). In particular, parameters involving the effects of chemistry (specifically dissociation and recombination) need to be taken into account. These consid-

*Graduate Research Assistant, GALCIT, California Institute of Technology, AIAA Student Member
†Visitor in Aeronautics, AIAA Member
‡Clarence L. Johnson Professor of Aeronautics, Director of GALCIT, AIAA Member
§Staff Engineer, Jet Propulsion Laboratory, AIAA Senior Member

erations directly affect the design of the experimental conditions and the subsequent interpretation of the experimental data. Table 1 lists the desired actual atmospheric flight conditions that needed to be modeled in these shock tunnel tests. These chemistry effects or so-called 'real gas effects' can only be correctly simulated by matching the stagnation enthalpy of the flow and the binary scaling parameter. This is something that cannot be achieved in typical 'cold' hypersonic flows which duplicate some of the relevant physical flow phenomena, but not the proper chemical phenomena. It is apparent that the effects of chemistry can only be observed in test flows that match the high flight velocities and consequently the high temperatures. Such flows are called 'hot' hypersonic flows or hypervelocity flows and can only be produced in high enthalpy facilities.

In ground test facilities, such as the T5 Hypervelocity Shock Tunnel used for these experiments, the flow is accelerated from a stationary, high–enthalpy reservoir, where the gas is in a significantly dissociated state, through a nozzle expansion. During this expansion much, but not all, of the dissociated gas recombines, so that some of the total enthalpy remains locked in the dissociation. In addition, the expansion is usually not taken to very high area ratios, so that the free stream temperature ($T_{\infty,tm}$) is higher than that in the real flow. Here, tm is an abbreviation for 'test model'. This results in a non-negligible freestream specific enthalpy as compared to the actual flight environment where the freestream temperature ($T_{\infty,fv}$) is typically quite low and consequently the specific static enthalpy ($h_{\infty,fv}$) is also quite low (where fv is an abbreviation for 'flight vehicle'). This mismatch in freestream enthalpy conditions is an indication that it is not valid to simply match the actual flight vehicle velocity ($U_{\infty,fv}$) with the test velocity ($U_{\infty,tm}$). Instead, an equivalent flight velocity is defined as $U_{eqv} = \sqrt{2\,h_{o,fv}}$ and is the relevant quantity that should be used when evaluating the Reynolds number for comparsion between experiments and flight data or computations. This ensures that the conditions in the region between the shock and the body are correctly simulated.

It is also important to recognize that the freestream dissociation in the shock tunnel causes the stagnation–point to freestream density ratio to be a little smaller than in real flight, where the freestream is undissociated. It is therefore better to use the density after an equilibrium normal shock (ρ'), rather than the freestream density (ρ_∞) when evaluating the Reynolds number. In reality, the equilibrium condition may not actually be achieved in the flow since the distance from the bow shock to the stagnation point may be significantly smaller than the characteristic dissociation length. Similarily, the viscosity should be evaluated at the temperature behind an equilibrium normal shock (T') which is the proper temperature for comparison purposes. Using the above arguments, the proper Reynolds number to be used when comparing the experimental test results with other data (either flight data or computations) should be:

$$Re' = \frac{\rho' U_{eqv} L}{\mu'},$$

where ρ' is the post-equilibrium-shock density, U_{eqv} is the equivalent flight velocity, L is the characteristic body length scale (taken to be the ballute ring cross-sectional radius), and μ' is the viscosity evaluated at the post-equilibrium-shock temperature. Table 2 summarizes the important quantities and reference Reynolds number (Re') relevant for the spacecraft missions under consideration. It also lists the Reynolds number evaluated at the freestream conditions (Re_∞) for comparison purposes.

3 Experimental Setup

3.1 T5 Hypervelocity Shock Tunnel

This series of experiments was performed in the GALCIT T5 Hypervelocity Free-Piston Shock Tunnel. In this reflected shock tunnel facility, a piston is initially launched by high pressure air. The resulting adiabatic compression of a helium-argon mixture bursts a diaphragm ($P_{burst} \simeq 90$ MPa) causing a shock wave to travel into a shock tube whose end wall is closed except for the small throat of the nozzle. The reflected shock from the end wall creates a quasi-constant pressure reservoir for the subsequent steady expansion through the nozzle. Shock speeds of up to 5 km/s can be obtained to produce nominal Mach 5 flows with a specific reservoir enthalpy of 25 MJ/kg, reservoir pressure of 60 MPa and reservoir temperature of 8000 K. Typical flow velocities are of the order of 3 to 6 km/s with typical useful test times ranging from 1 to 2 ms. Existing shock tunnel diagnostic instrumentation provides the shock speed and reservoir pressure from which the freestream conditions can be calculated. The data acquisition system consisted of three DSP Technology CAMAC crates with 52 channels available for acquiring data from model instrumentation. Detailed descriptions regarding T5 operations, flow calibration and flow quality can be found in Hornung[8].

3.2 Model and Instrumentation

The model consisted of two pieces. A stainless steel ring which represented the actual ballute in flight and a small ball bearing located in front of the ring to represent the spacecraft. The ballute ring had a cross-sectional diameter of 20 mm and a nominal diameter of 140 mm (*i.e.*, ID = 120 mm, OD = 160 mm). A portion of the ballute ring consisted of a removable instrument plate to allow for installation of the thermocouple gauges. The spacecraft had a diameter of 15.9 mm and was held in place by an axial sting mounting that protruded through the ballute ring from the main sting support. The spacecraft was located 62 mm in front of the ballute (measured from the center of the spacecraft to the midsection of the ring) for the first series of tests and was located 93 mm in front of the ballute for the second series of tests. There was no noticeable difference between the heat transfer results for the two configurations. The model was aligned with the axis of the tunnel and was tested at $0^\circ \pm 0.1^\circ$ angle of attack.

The ballute ring was instrumented with 11 flush-mounted thermocouples placed in 5° increments in the azimuthal direction and 15° increments in the cross-sectional direction (*i.e.* ranging from -75° to 75° with negative angles representing the inside of the ring, 0° representing the windward line and positive angles representing the outside of the ring). Refer to Figure 1 for a schematic drawing of the instrument layout. In addition, one thermocouple was located at the stagnation point of the spacecraft.

The small (0.8 mm diameter) and fast response (1 μs) coaxial Type E thermocouples were manufactured in-house based on a modified design originally developed by Sanderson[12] and whose performance was tested in detail by Davis[2]. During the shot, the thermocouple signal was amplified by a factor of 500 and then sampled at 200 kHz. The sampled voltage levels were converted to temperature using correlations for Type E thermocouples. The heat flux for each thermocouple was subsequently computed using a spectral deconvolution technique based on the heat equation for 1D unsteady heat transfer in a semi-infinite solid. Refer to Davis[2] for details on this analysis.

3.3 Test Section Setup

The model was mounted on a sting and aligned with the axis of the tunnel. It was positioned such that the nozzle exit plane was approximately 30 mm in front of the spacecraft during the shot. Refer to Figure 2 for a photograph of the model mounted in the test section. The 7 ° half-angle conical nozzle was used for these experiments since it produces reasonably uniform flow properties across a wide range of test conditions. To achieve the low densities for these experiments, two different throats were used (15 mm and 7 mm diameter) resulting in nozzle area ratios of 438 and 2012, and nominal Mach numbers of 7 and 10. The differing Mach numbers had no observable effect on the measured heat flux results. Since the conical nozzle results in a diverging flow so that freestream conditions vary with downstream distance, it is important to note that the freestream conditions used to calculate the Reynolds number and Stanton number were evaluated at the plane of the ballute ring. Care was also taken to ensure that the model was within the core flow and not affected by the expansion fan from the nozzle exit. The optical window was placed such that the entire model was visible within the field of view.

3.4 Flow Visualization

At the low densities desired for the test conditions, standard shadowgraphy was not sensitive enough to capture the major flow features. For this reason, it was necessary to seed the flow with sodium and tune the frequency of the dye laser used as the light source to one of the sodium D-lines. This was accomplished by spraying salt water on the shock tube endwall and allowing the water to evaporate. This would then leave salt crystals in the reservoir region which would vaporize and dissociate, seeding the flow with atomic sodium during the shot. A 'resonantly enhanced shadowgraph' was obtained for each of the carbon dioxide and nitrogen shots. No clear shadowgraphs could be obtained for the hydrogen shots because the extremely low densities and reservoir temperatures were too low to vaporize and dissociate the salt.

4 Results and Analysis

A total of 13 shots were carried out in carbon dioxide, 7 shots were performed in nitrogen and 7 shots were performed in hydrogen. The CO_2 shots were performed with reservoir pressures ranging from 5 MPa to 30 MPa and specific reservoir enthalpies ranging from 12 MJ/kg to 23 MJ/kg. The nitrogen shots were performed with nominal reservoir pressures from 4 MPa to 10 MPa and nominal specific reservoir enthalpy from 23 MJ/kg to 26 MJ/kg. The hydrogen shots were performed with reservoir pressures from 3 MPa to 25 MPa and specific enthalpies

ranging from 27 MJ/kg to 80 MJ/kg. The data collected for each shot consisted of a resonantly enhanced shadowgraph and heat flux data from each thermocouple. As indicated previously, the first series of experiments were performed with the spacecraft placed 62 mm in front of the ballute, while a second series of experiments were performed with the spacecraft placed 93 mm in front of the ballute. No measurable difference in the surface heat flux was observed, and all data from both series of experiments are presented on the same figures. The complete data set can be found in Rasheed *et al.*[11] and Fujii *et al.*[5].

Figure 3 shows a summary plot of the non-dimensional enthalpy (normalized by dissociation energy of the test gas) versus the post-equilibrium-shock Reynolds number and can be used to determine how well the experiments matched the similarity criteria for the actual missions. It can be seen that the carbon dioxide and nitrogen test conditions match very well with the Mars Micro Satellite and Titan Explorer missions, respectively. In both cases, the Reynolds number was matched. In addition, the enthalpy criteria was matched for the Mars mission and it was fairly close for the Titan mission. It can be seen that the hydrogen tests matched the Reynolds number, however they failed to match the enthalpy similarity criteria and care must be taken when extending the results of the present experiments to the Neptune Orbiter mission.

4.1 Description of Flow Field

Figure 4a is a resonantly enhanced shadowgraph taken during shot 2019 and shows the major flow features of the intended design condition for the ballute concept. For this configuration, the bow shock in front of the spacecraft passes through the ring ballute. The interaction of the spacecraft bow shock and the ring ballute bow shock occurs harmlessly in the region behind the ballute. This interaction can be seen just downstream of the ring in the bottom half of the picture. Waves that travel around the front circumference of the ring ballute can be seen along the front surface of the ring on the top half of the image (just opposite the top support structure). The smearing effect along the front surface of the ring which is more pronounced at the top and bottom edges is the self–luminosity of the gas in the high–enthalpy stagnation region. Peak heating rates are to be expected at the stagnation points on the spacecraft and on the ring ballute. One of the concerns about the relative axial location of the spacecraft and ballute is that the flow may become unsteady when the interaction between the two shock waves moves radially outward. Figure 4b is a resonantly enhanced shadowgraph taken from the second series of experiments during shot 2145 with the spacecraft moved further forward with respect to the ballute. The bow shock from the spacecraft is still 'swallowed' by the ballute ring, indicating that the ballute is still operating within its intended design envelope.

Flow fields quite different from the one described above would occur if the spacecraft bow shock would envelope the ring ballute (*i.e.* the entire ring fell inside the the spacecraft bow shock). Another very undesirable condition could occur if the the spacecraft bow shock impacted the ring. This would result in very high heating rates due to the shock-on-shock interaction. The above two scenarios could occur at lower Mach numbers (where the bow shock is less slender) or if the distance between the spacecraft and the ring ballute was increased sufficiently. Another completely different flow field would be generated if the hole in the ring ballute were blocked. Such situations would need to be understood and characterized before the ballute concept could be validated for actual use on a flight vehicle.

4.2 Theoretical Heat Flux

The theoretical heat flux can be estimated using the theory developed by Fay and Riddell[4] and summarized by White[13]. The resulting expression for stagnation point heat flux on a cylinder is:

$$\dot{q} = 0.570\, Pr^{-0.6} \sqrt{\rho_e \mu_e K} \left(\frac{\rho_w \mu_w}{\rho_e \mu_e} \right)^{0.1} (h_e - h_w),$$

where Pr is the Prandtl number, ρ_e is the boundary layer edge density, μ_e is the viscosity evaluated at edge temperature, K is the stagnation–point velocity gradient, ρ_w is the density at the wall, μ_w is the viscosity evaluated at the wall temperature, h_e is the boundary–layer edge enthalpy and h_w is the enthalpy at the wall. In this case, the edge conditions are to be interpreted as the inviscid stagnation conditions. The expression for stagnation point heating on a sphere is the same as the above where the constant 0.570 is replaced by 0.763.

The quantity $C_w = \rho_w \mu_w / \rho_e \mu_e$ is known as the Chapman-Rubesin parameter and is used as a correction factor to take into account compressibility effects. As noted by White, the use of this parameter is suitable for adiabatic walls, but is not very good for hot or cold walls. This is corrected by evaluating $C^* = \rho^* \mu^* / \rho_e \mu_e$ at the reference temperature, T^*, determined empirically by Eckert[3] as

$$\frac{T^*}{T_e} \approx 0.5 + 0.22\frac{\gamma-1}{2}\sqrt{Pr}M_e^2 + 0.5\frac{T_w}{T_e},$$

where the subscript e denotes boundary layer edge conditions. For the purposes of stagnation point calculations, the stagnation conditions can be substituted for the edge conditions in the above equation. In fact, for a stagnation point, the second term is zero and in the case of the T5 experiments, the ratio T_w/T_o is approximately zero. Eckert's reference temperature formula then collapses to:

$$\frac{T^*}{T_e} \approx 0.5.$$

Furthermore, White noted that, for gases:

$$C^* = \frac{\rho^*\mu^*}{\rho_o\mu_o} \approx \left(\frac{T^*}{T_e}\right)^{-1/3},$$

thereby reducing to a constant $C^* \approx 0.5^{-1/3}$. Also, as described by White, the stagnation velocity gradient, K, can be estimated using Newtonian theory:

$$\frac{KD}{V_\infty} \approx \sqrt{\frac{8\rho_\infty}{\rho_e}},$$

where D is the diameter of the cylindrical or spherical nose of the body. Once again, the edge conditions in the above equations should be the stagnation conditions. Finally, recognizing that h_w is negligible, the equation for stagnation point heat flux on a cylinder reduces to:

$$\dot{q} = 0.570\, Pr^{-0.6}\sqrt{\rho_o\mu_o K}\, C^{*0.1}h'_o,$$

As before, the expression for a sphere is the same as above with the constant 0.570 replaced by 0.763.

4.3 Calculation of Stanton Number and Reynolds Number

As discussed in Section 2, the relevant Reynolds number for these flows is:

$$Re' = \frac{\rho' U_{eqv} L}{\mu'},$$

where ρ' is the reference density, U_{eqv} is the equivalent velocity, L is the characteristic body length scale (taken to be the ballute ring cross-sectional radius) and μ' is the viscosity evaluated at the reference temperature. Viscosities were calculated using a simple code based on a viscosity model for reacting gases developed by Blottner et al.[1] in order to determine the viscosity of each species in the gas mixture at the reference temperature. Coefficients for the model for the different gases were obtained from Olynick et al[10]. Using the computed gas composition at the reference condition, the code then used Wilke's[14] semi-empirical mixing rule to calculate the overall viscosity of the gas mixture.

The Stanton number used to non-dimensionalize the heat flux data was computed as:

$$St' = \frac{\dot{q}}{\rho' U_{eqv} h'_o},$$

where $\dot{q}$ represents the dimensional heat flux, ρ' and U_{eqv} are as before and h'_o is the total enthalpy behind the equilibrium normal shock. Note that the total enthalpy before and after the shock are the same as a result of conservation of energy, so that h'_o and h_o are equivalent. The uncertainty for the experimental Stanton numbers is about ±20%.

4.4 Mars Micro Satellite

Figure 5 shows a summary plot of the St' versus Re' for the carbon dioxide shots used to simulate the Mars mission. The plot shows that the theoretical estimates for the heat flux are in very good agreement with experimentally measured values. Furthermore, the expected $Re^{-0.5}$ power-law for heat flux in a laminar boundary layer is seen to hold over an order-of-magnitude in Reynolds number.

4.5 Titan Organics Explorer

Figure 6 is a resonantly enhanced shadowgraph obtained from shot 2021 showing the same relevant flow features as was observed in the carbon dioxide shots and described in section 4.1. Figure 7 shows the summary plot of the St' versus Re' for the nitrogen shots used to simulate the Titan Explorer mission. As with the carbon dioxide plot, it shows very good agreement between the theoretical estimates and the experimentally measured values for heat flux. In addition, the plot also shows that the $Re^{-0.5}$ power-law holds over an order-of-magnitude.

4.6 Neptune Orbiter

Figure 8 shows the summary plot of the St' versus Re' for the hydrogen shots used to simulate the Neptune Orbiter mission. Although no useful pictures

were obtained for these shots due to the extremely low densities and enthalpies, one would expect flowfields similar to those observed in the carbon dioxide and nitrogen shots. It should be noted, however, that these shots are very far from achieving similarity with the real flow of the Neptune orbiter because the velocity in T5 is at least a factor of 3 smaller than the real velocity. The real–gas effects in hydrogen at the conditions tested in T5 are restricted to vibrational excitation, while the enthalpy in the real flow is high enough to cause significant dissociation. These results must therefore not be used to extrapolate to the real flow.

4.7 Unsteady Flows

As mentioned earlier, computations suggested that situations could arise where unsteady flows could occur. For this reason, a few shots were performed in order to gain a preliminary understanding of these flow regimes and to validate the computations in a qualitative sense. In particular, tests were performed to examine the configuration in which the hole of the ring ballute was completely blocked using an aluminum plate of 3 mm thickness. Figure 9 shows nitrogen flow over the model with the ring blocked by an aluminum plate. As may be seen, the bow shock of the spacecraft is very irregular. Such shock shapes are not able to exist in steady flows. The configuration of the shock is also qualitatively similar to one phase of the computed unsteady flows. It may be concluded that this is an unsteady flow that results from the interaction of the spacecraft shock with the ballute shock.

5 Conclusions

By extending the range of operation of the T5 Hypervelocity Shock Tunnel to lower pressure, it has been possible to make useful simulations of the flow over a model of a spacecraft with a toroidal ballute in situations corresponding to aerocapture of the Mars Micro Satellite and the Titan Organics Explorer. They are useful since they permit extrapolation to the flight Reynolds number with reasonable confidence. Tests performed in hydrogen to simulate flows relevant to the Neptune Orbiter were too far from the flight total enthalpy and should be used with caution. The tests confirmed that a toroidal ballute can avoid the unsteadiness encountered with simply connected ballute flows. The fact that such unsteadiness does occur was also substantiated.

Acknowledgements

This work was jointly funded by the Mars and Outer Planets Exploration Technology Programs at the Jet Propulsion Laboratory, California Institute of Technology, under a contract with the National Aeronautics and Space Administration.

References

[1] F.G. Blottner, M. Johnson, and M.G. Ellis. Chemically reacting viscous flow program for multi-component gas mixtures. Technical Report SC-RR-70-754, Sandia Laboratories, Albuquerque, N.M., December 1971.

[2] J.P. Davis. *High-Enthalpy Shock/Boundary-Layer Interaction on a Double Wedge*. PhD thesis, California Institute of Technology, 1999.

[3] E.R.G. Eckert. Engineering relations for friction and heat transfer to surfaces in high velocity flow. *Journal of the Aeronautical Sciences*, 22:585–587, August 1955.

[4] J. Fay and F.R. Riddell. Theory of stagnation point heat transfer in dissociated air. *Journal of the Aeronautical Sciences*, 25(2):73–85, February 1958.

[5] K. Fujii, A. Rasheed, B. Valiferdowsi, and H.G. Hornung. Preliminary experimental investigation of the flow over a toroidal ballute - Extending to lower Reynolds number range. Technical Report FM 01-1, GALCIT, California Institute of Technology, 2001.

[6] J.L. Hall. A review of ballute technology for planetary aerocapture, 2000. (4th IAA Conference on Low Cost Planetary Missions, May 2-5, Laurel, MD, USA).

[7] J.L. Hall and A.K. Le. Aerocapture trajectories for spacecraft with large, towed ballutes. AAS/AIAA Paper 01-235, 2001. (AAS/AIAA Space Flight Mechanics Meeting, February 11-15, San Diego, CA, USA).

[8] H.G. Hornung. Performance data of the new free-piston shock tunnel T5 at GALCIT. AIAA Paper 92-3943, 1992. (17th Aerospace Ground Testing Conference, July 6-8, Nashville, TN, USA).

[9] H.G. Hornung. Hypersonic flow over bodies in tandem and its relevance to ballute design. AIAA Paper 2001-2776, 2001. (31st AIAA Fluid Dynamics Conference and Exhibit, June 11-14, Anaheim, CA, USA).

[10] D. Olynick, Y.-K. Chen, and M. Tauber. Aerothermodynamics of the stardust sample return capsule. *Journal of Spacecraft and Rockets*, 36(3):442–462, 1999.

[11] A. Rasheed, K. Fujii, B. Valiferdowsi, and H.G. Hornung. Preliminary experimental investigation of the flow over a toroidal ballute. Technical Report FM 00-4, GALCIT, California Institute of Technology, 2000.

[12] S.R. Sanderson. *Shock Wave Interaction in Hypervelocity Flow*. PhD thesis, California Institute of Technology, 1995.

[13] F.M. White. *Viscous Fluid Flow*. McGraw-Hill, Inc., second edition, 1991.

[14] C.R. Wilke. A viscosity equation for gas mixtures. *Journal of Chemical Physics*, 18(4):517–519, April 1950.

Table 1: Ballute mission design parameters.

	Mars Micro Satellite	Titan Organics Explorer	Neptune Orbiter
Ring Diameter (m)	15	52	140
Cross Sectional Diameter (m)	3	13	40
Velocity (m/s)	5490	8550	26900
Density (kg/m^3)	7.1×10^{-7}	1.9×10^{-7}	6.0×10^{-9}
Gas	95% CO_2	98% N_2	80% H_2

Table 2: Relevant scaling parameters for the ballute missions under consideration.

	Mars Micro Satellite	Titan Organics Explorer	Neptune Orbiter
h_o (MJ/kg)	15.1	36.6	361.8
U_{eqv} (m/s)	5490	8550	26900
ρ' (kg/m^3)	1.8×10^{-5}	4.7×10^{-6}	6.7×10^{-8}
Re'	1400	1700	570
Re_∞	650	760	490

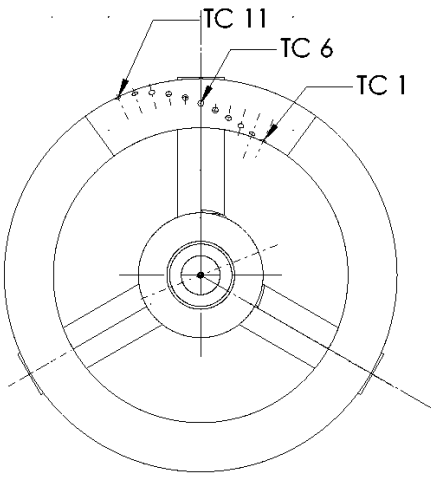

Figure 1: Front view of the ballute model showing the thermocouple layout on the ballute ring. Thermocouple 1 (TC 1) is on the inside of the ring at the -75° position, thermocouple 6 (TC 6) is at the stagnation point (0°) and thermocouple 11 (TC 11) is on the outside of the ring at the 75° position. Each thermocouple is separated by 5° in the azimuthal direction. Not shown is thermocouple 12 which is on the stagnation point of the spacecraft.

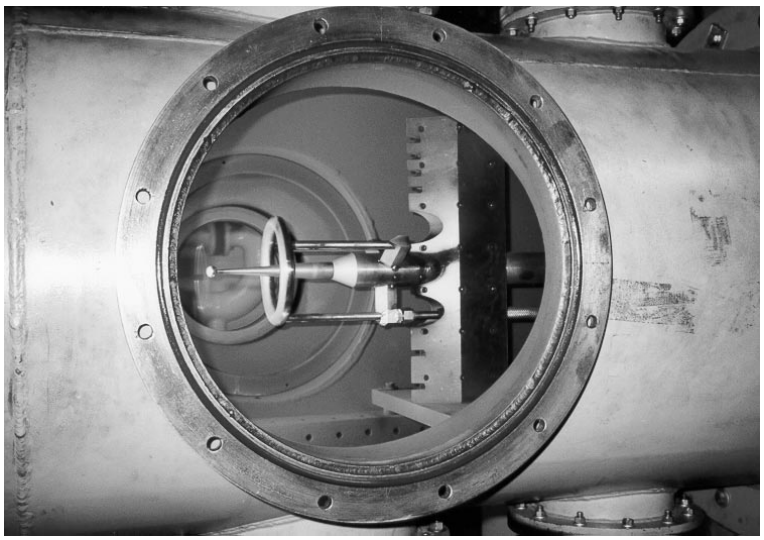

Figure 2: Photograph of the model in the test section.

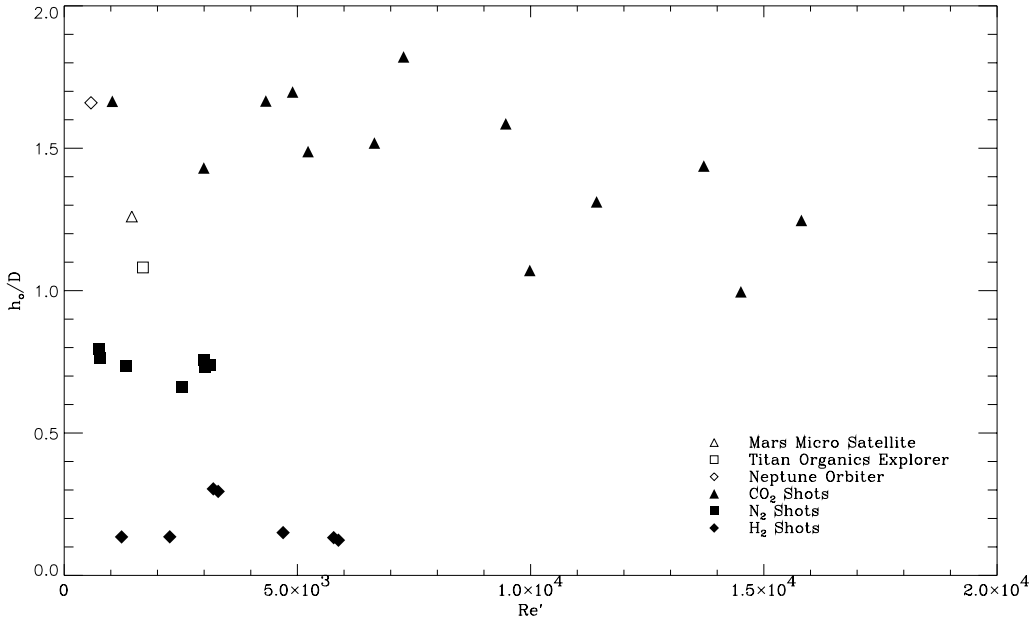

Figure 3: Plot of stagnation enthalpy normalized by the test gas dissocation energy (h_o/D) versus post-equilibrium-shock Reynolds number (Re') for all the shots (solid symbols). The triangles are for the CO_2 shots, the squares are for the N_2 shots, and the diamonds are for the H_2 shots. The open symbols represent the design points of the missions being simulated.

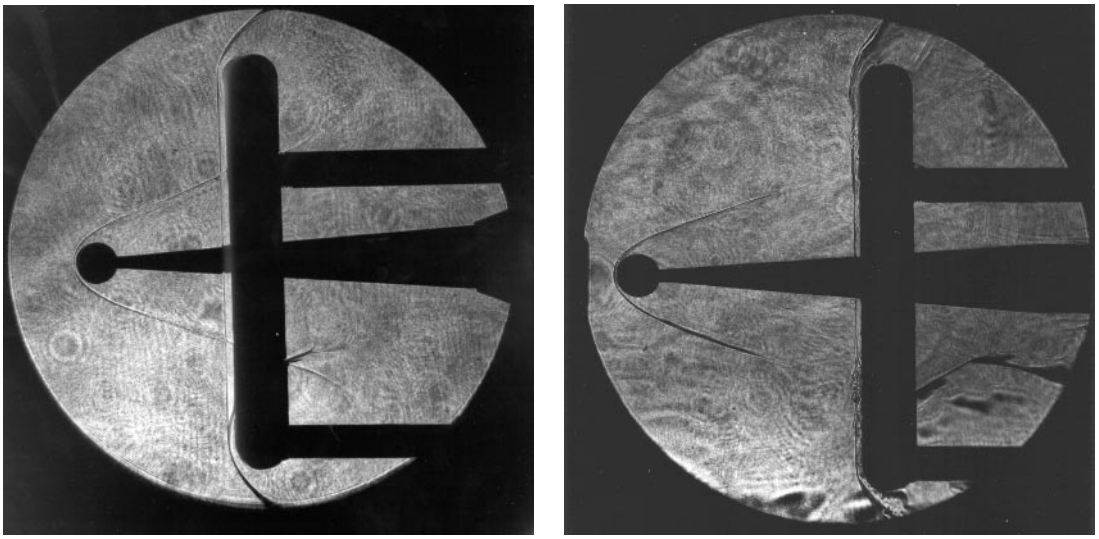

(a) (b)

Figure 4: (a) Resonantly enhanced shadowgraph showing the relevant flow features around the ballute and spacecraft for (a) shot 2019 (CO_2, 17.7 MJ/kg) with the spacecraft 62 mm in front of the ballute ring and (b) shot 2145 (CO_2, 20.4 MJ/kg) with the spacecraft 93 mm in front of the ballute ring. The distances were measured from center of the spacecraft to the center of the ballute ring.

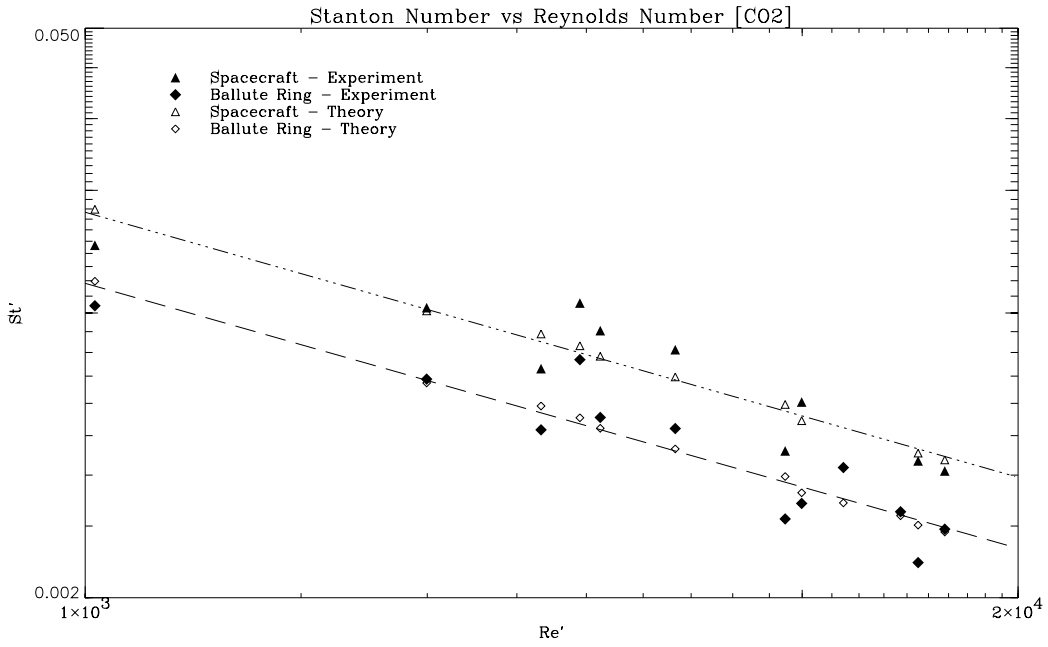

Figure 5: Plot of St' versus Re' for the CO_2 shots. The triangles represent measurements at the stagnation point of the spherical spacecraft, and the diamonds are measurements on the stagnation line of the toroidal ballute. Filled symbols represent the experimental data, and the open symbols are the theoretical estimates. The lines represent linear fits of the experimental data while enforcing the $Re^{-1/2}$ power law for heat flux in a laminar boundary layer. The triple-dashed dotted and dashed lines are for the spacecraft stagnation and ballute, respectively.

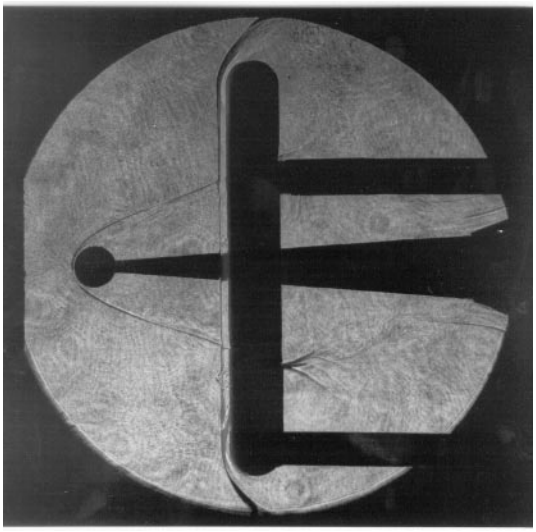

Figure 6: Resonantly enhanced shadowgraph showing the relevant flow features around the ballute and spacecraft for shot 2021 (N_2, $h_o = 22.1$ MJ/kg).

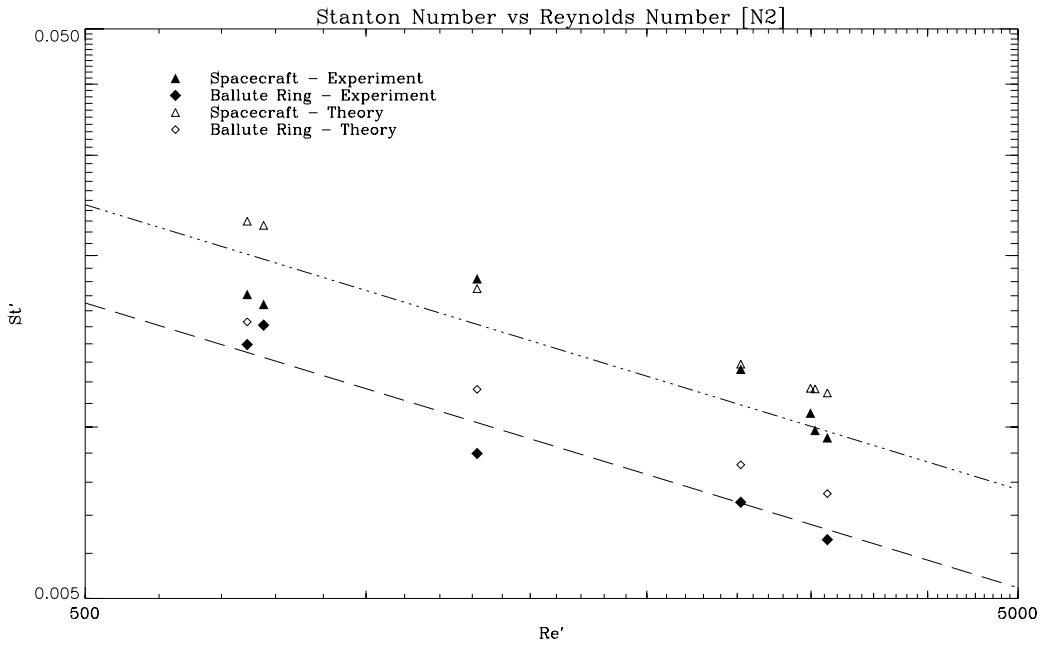

Figure 7: Plot of St' versus Re' for the N_2 shots. Symbols and lines are the same as in Figure 5.

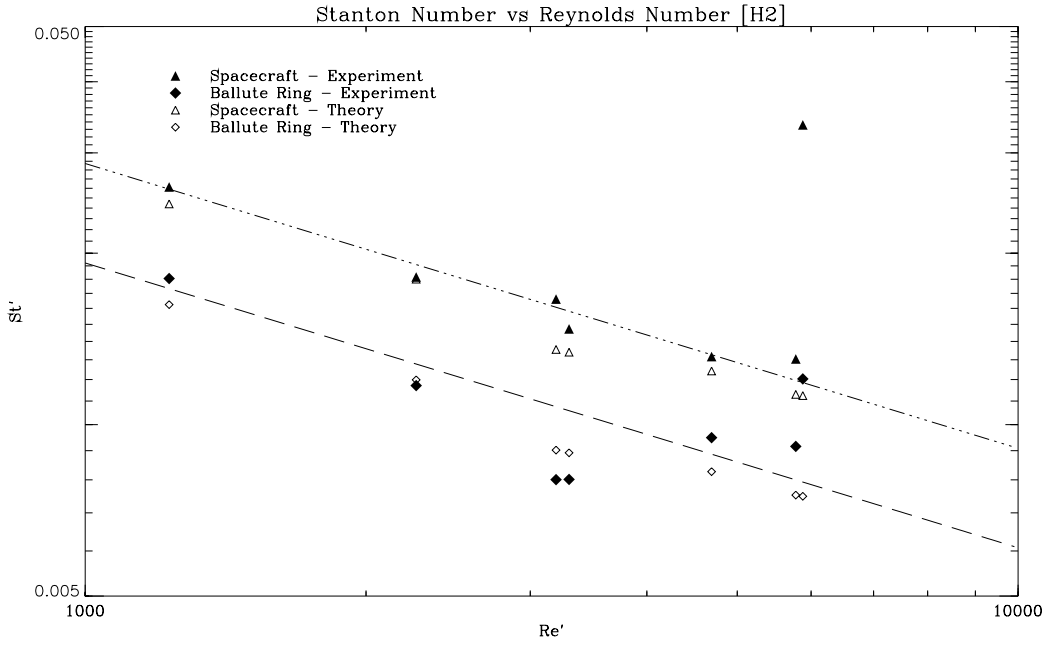

Figure 8: Plot of St' versus Re' for the H_2 shots. Symbols and lines are the same as in Figure 5. This data is to be used with caution since the T5 tests were very far from achieving similarity with the actual expected flight conditions.

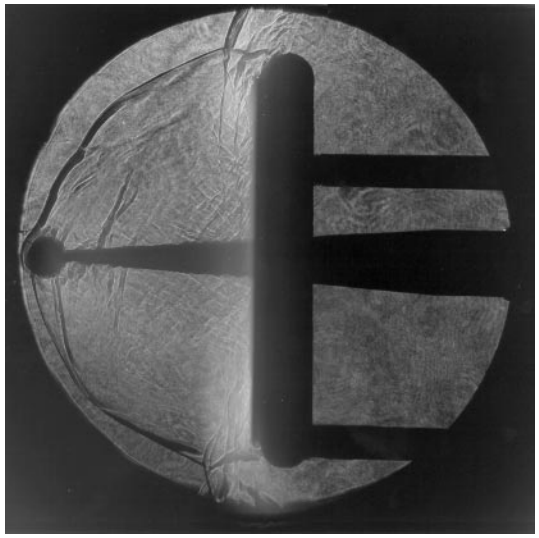

Figure 9: Resonantly enhanced shadowgraph showing the relevant flow features around the ballute and spacecraft when the ring is blocked by an aluminum plate (N_2, $h_o = 25.6$ MJ/kg). Note the irregular bow shock of the spacecraft. This clearly results from the interaction between the spacecraft and ballute shocks, which causes violent unsteadiness.